

Cite this: *Phys. Chem. Chem. Phys.*, 2012, **14**, 10140–10146

www.rsc.org/pccp

The phase diagram of water from quantum simulations

Carl McBride,^a Eva G. Noya,^b Juan L. Aragones,^a Maria M. Conde^a and Carlos Vega^{*a}

Received 26th March 2012, Accepted 22nd May 2012

DOI: 10.1039/c2cp40962c

The phase diagram of water has been calculated from the TIP4PQ/2005 model, an empirical rigid non-polarisable model. The path integral Monte Carlo technique was used, permitting the incorporation of nuclear quantum effects. The coexistence lines were traced out using the Gibbs–Duhem integration method, once having calculated the free energies of the liquid and solid phases in the quantum limit, which were obtained *via* thermodynamic integration from the classical value by scaling the mass of the water molecule. The resulting phase diagram is qualitatively correct, being displaced to lower temperatures by 15–20 K. It is found that the influence of nuclear quantum effects is correlated to the tetrahedral order parameter.

1 Introduction

Ever since the monumental work undertaken by Bridgman in 1912¹ there has been intense and continued interest in the phase diagram of water.^{2,3} The prediction of the phase diagram serves as a severe test for any model of water.^{4,5} Although the first computer simulations of water were performed in 1969 by Barker and Watts⁶ and in 1971 by Rahman and Stillinger,⁷ the calculation of the complete phase diagram was only recently undertaken, using the classical models TIP4P and SPC/E.⁸ Although the TIP4P model provided a qualitatively correct phase diagram, there was room for improvement (*i.e.* the melting point of ice I_h was situated at around 230 K). Consequently a new re-parameterisation, named TIP4P/2005, was proposed⁹ leading to a satisfactory description of a number of properties of water.^{10,11} The TIP4P/2005 model is a rigid non-polarisable model designed for classical simulations. In an indirect fashion TIP4P/2005 implicitly incorporates nuclear quantum effects, at least at moderate to high temperatures. However, the model fails when it comes to describing the equation of state at low temperatures¹² or C_p .¹³ The origin of the failure is the use of classical simulations to describe the properties of water. Quantum effects are present in water^{14–19} even at “high” temperatures, due to the particularly small moment of rotational inertia, engendered by the low mass of hydrogen, in conjunction with the relatively high strength of the intermolecular hydrogen bonds.

Nuclear quantum effects can be incorporated into condensed matter simulations *via* the path integral technique

proposed by Feynman²⁰ (for an excellent review see ref. 21). Barker²² and Chandler and Wolynes²³ showed that the formalism of Feynman is equivalent, or “isomorphic”, to performing classical simulations of a modified system where each molecule is replaced by a polymeric ring composed of P beads. The TIP4P/2005 model, successful for classical simulations,^{24,25} was recently adjusted for use in such quantum simulations (the charge located on the hydrogen atom was increased by $0.02e$ so as to maintain the same internal energy in a quantum simulation as the TIP4P/2005 model in a classical simulation) becoming the TIP4PQ/2005 model.¹² This new variant of TIP4P/2005 has been successful in describing the temperature of maximum density²⁶ of water and heat capacities.¹³ It is for this model that we calculate the phase diagram.

2 Methods

2.1 Path integral Monte Carlo

The partition function, Q_{NpT} , for a system of N rigid molecules in the NpT ensemble is given (except for an arbitrary pre-factor that renders Q_{NpT} dimensionless) by $Q_{NpT} = \int \exp(-\beta pV) Q_{NVT} dV$. In the NVT ensemble Q_{NVT} is given by:

$$\frac{1}{N!} \left(\frac{MP}{2\pi\beta\hbar^2} \right)^{\frac{3NP}{2}} \int \prod_{i=1}^N \prod_{t=1}^P \rho_{\text{rot},i}^{t,t+1} \left(\frac{\beta}{P}, \omega_i^t \omega_i^{t+1} \right) dr_i^t d\omega_i^t \times \exp \left(-\frac{MP}{2\beta\hbar^2} \sum_{i=1}^N \sum_{t=1}^P (r_i^t - r_i^{t+1})^2 - \frac{\beta}{P} \sum_{t=1}^P U^t \right) \quad (1)$$

where P is the number of Trotter slices or “replicas” through which nuclear quantum effects are introduced (for $P = 1$ the simulations become classical). Each replica, t , of molecule i interacts with the replicas with the same index t of the

^a Departamento de Química Física, Facultad de Ciencias Químicas, Universidad Complutense de Madrid, 28040 Madrid, Spain. E-mail: cvega@quim.ucm.es

^b Instituto de Química Física Rocasolano, Consejo Superior de Investigaciones Científicas, CSIC, Calle Serrano 119, 28006 Madrid, Spain

remaining particles *via* the inter-molecular potential U , and interacts with replicas $t - 1$ and $t + 1$ of the same molecule i through a harmonic potential (connecting the centre of mass of the replicas) whose coupling parameter depends on the mass of the molecules (M) and on the temperature ($\beta = 1/k_B T$), and through a term ($\rho_{\text{rot},i}^{t,t+1}$), named the rotational propagator, that incorporates the quantisation of the rotation and which depends on the relative orientation of replicas t and $t + 1$. Pioneering work was undertaken by Wallqvist and Berne,²⁷ and by Rossky and co-workers²⁸ who used an approximate expression for the rotational propagator of an asymmetric top (*i.e.* water). Another technique is that of the stereographic projection path integral²⁹ which has been used to study TIP4P clusters.³⁰ In 1996 Müser and Berne³¹ provided an expression of the rotational propagator for spherical and symmetric top molecules. Quite recently the authors have extended the expression of Müser and Berne to the case of an asymmetric top,³² which is the case of water. The propagator is a function of the relative Euler angles between two contiguous beads and of PT . The internal energy E can be calculated through the derivative of the logarithm of Q_{NVT} with respect to β , and is given by the sum of the kinetic and potential energy terms, $E = K_{\text{translational}} + K_{\text{rotational}} + U = K + U$. A more complete account concerning path integral Monte Carlo simulations of rigid rotors, and their application to water, can be found in the article by Noya *et al.*³³

2.2 Phase diagram calculation

The determination of the phase diagram of the quantum system is undertaken in several steps. First the classical phase diagram of the TIP4PQ/2005 model was calculated. To do this, for each solid phase a reference thermodynamic state is chosen and the free energy of the classical system is determined using either the Einstein crystal³⁴ or the Einstein molecule methodologies.³⁵ For the fluid phase the free energy of the classical system is determined at a reference state by transforming the TIP4PQ/2005 model into the Lennard-Jones model, for which the free energy is well known.³⁶ The free energy of the classical system under distinct thermodynamic conditions can be obtained *via* thermodynamic integration. This permits one to determine an initial coexistence point of the classical system for each phase transition by imposing the usual condition of equal chemical potential for a given T and p . Gibbs–Duhem simulations³⁷ are then performed to trace out the complete phase diagram. The procedure has been described in detail in ref. 38. At the end of this first step the phase diagram of the classical system is known.

In the second step the chemical potential of the quantum system is determined at a reference thermodynamic state, again for each phase of interest. It is worth describing this procedure in some detail. Let us define the excess quantum free energy as the free energy difference between the quantum system and its classical counterpart at the same T and p :

$$G^{\text{ex},Q} = G - G^{\text{classical}} \quad (2)$$

Thus the free energy of the quantum system, G , can be obtained if the classical and excess contributions are known. The free energy of the classical system was determined in

the first step, so we shall now focus on the evaluation of $G^{\text{ex},Q}$. One defines a parameter, λ , whose purpose is to scale the mass of the atoms of the molecule of water such that: $m_{\text{O}} = \lambda m_{\text{O},0} = m_{\text{O},0}/\lambda'$ and $m_{\text{H}} = \lambda m_{\text{H},0} = m_{\text{H},0}/\lambda'$, where $m_{\text{O},0}$ and $m_{\text{H},0}$ are the masses of O and H in the molecule of water, where $\lambda' = 1/\lambda$. Thus one can slide from the quantum limit (for which $\lambda' = 1$) to the classical limit (for which $\lambda' = 0$) by simply changing the λ' parameter. From the relationship $G = -kT \ln Q_{NpT}$ the derivative of the free energy with respect to λ' can be calculated,³⁹ obtaining:

$$\frac{\partial(G/NkT)}{\partial\lambda'} = \frac{1}{\lambda'} \left\langle \frac{K}{NkT} \right\rangle \quad (3)$$

This is due to the fact that when the masses of all atoms of the molecule are scaled by a factor $1/\lambda'$ the total mass, M , is also scaled by a factor $1/\lambda'$. The same is true for the eigenvalues of the inertia tensor and thus the energies of the asymmetric top appearing in the rotational propagator are also scaled by a factor λ' . The average of the value in the angled brackets should be performed for the value of λ' of interest. By using eqn (3) in conjunction with the fact that the total kinetic energy (with the translational and rotational contributions) is $3NkT$ for the classical and for the quantum system in the limit of infinitely heavy molecules, it can be shown that the chemical potential of the quantum system μ can be obtained from the expression:

$$\frac{\mu}{kT} = \frac{G^{\text{classical}}}{NkT} + \int_0^1 \frac{1}{\lambda'} \left[\left\langle \frac{K}{NkT} \right\rangle - 3 \right] d\lambda' \quad (4)$$

To determine the integral of eqn (4) (*i.e.* $G^{\text{ex},Q}/NkT$) it is sufficient to perform simulations at decreasing values of λ' , to determine the integrand for each considered value of λ' and subsequently implement a numerical procedure to estimate the value of the integral. It follows from eqn (4) that the difference in chemical potential in the quantum system between two phases, $\Delta\mu = \mu_{\text{B}} - \mu_{\text{A}}$, can be obtained as:

$$\frac{\Delta\mu}{kT} = \frac{\Delta\mu^{\text{classical}}}{kT} + \int_0^1 \frac{1}{\lambda'} \left[\left\langle \frac{K_{\text{B}}}{NkT} \right\rangle - \left\langle \frac{K_{\text{A}}}{NkT} \right\rangle \right] d\lambda' \quad (5)$$

This expression states that the difference in chemical potential between two phases is simply the value of the difference in the classical system plus a correction term that accounts for the difference in the quantum excess free energies. Thus, after the second step one knows either the chemical potential of the quantum system at a reference state, or similarly the difference in chemical potential between two phases, again at a reference state.

The third step in the determination of the phase diagram of the quantum system requires the determination of one initial coexistence point for each coexistence line. By using thermodynamic integration,³⁸ the free energy of each phase of the quantum system is determined as a function of T and p . This provides the location of at least one coexistence point between each pair of phases by imposing the condition of identical chemical potential, p and T between the two phases.

The fourth and final step is the tracing out of the complete coexistence lines thus yielding the phase diagram. This is done by using the Gibbs–Duhem simulations, starting from the initial coexistence point determined at the end of the third step.

2.3 Simulation details

The expression of the rotational propagator is given in ref. 32. The propagator is composed of an infinite sum over the energy levels of the free asymmetric top rotor. In practice the summations are truncated; we adopted the criterion that the propagator had converged when the absolute difference between the value of the propagator for two consecutive values of J (normalised so that $\rho(0,0,0) = 1$ for both values of J) is less than 10^{-6} per point. A grid of one degree for each Euler angle was used, and results for intermediate angles were obtained by interpolation. Simulations consisted of 360 molecules for liquid water, 432 molecules for ices I_h and II, 324 molecules for ice III, 504 for ice V and 360 for ice VI. The algorithm of Buch *et al.*⁴⁰ was used to obtain a proton disordered configuration of ices I_h, III, V and VI simultaneously having zero dipole moment and at the same time satisfying the Bernal–Fowler rules.^{41,42} For ice III we additionally imposed the condition that the selected proton disordered configuration presented an internal energy that lies in the centre of the energy distribution shown in Fig. 2 of ref. 43. Direct I_h–fluid coexistence simulations used about 1000 molecules for the classical system and about 600 for the quantum one. Free energies of the classical system were obtained using the Einstein molecule methodology for a given proton disordered configuration and subsequently adding the Pauling⁴² entropy contribution ($-RT \ln(3/2)$). The methodology has been described in detail elsewhere.³⁸ The Lennard-Jones part of the potential was truncated at 8.5 Å and long ranged corrections were added. Coulombic interactions were treated using Ewald sums. For the solid phase anisotropic NpT Monte Carlo simulations were performed in which each of the sides of the simulation box were allowed to fluctuate independently. The number of replicas P in the path integral simulations was selected for each temperature by imposing that PT be approximately 1900 ± 300 . This choice guarantees that, for a rigid model of water, the thermodynamic properties are within two per cent of the value obtained as P tends to infinity. In general the simulations of this work consisted of 200 000 Monte Carlo cycles, where a cycle consists of a trial move per particle (the number of particles is equal to NP where N is the number of water molecules) plus a trial volume change in the case of NpT simulations. To increase the accuracy, in the determination of the excess quantum free energies, four independent runs were performed for each value of λ' . In eqn (5) $\Delta\mu^{\text{classical}}$ is zero if evaluated at the coexistence T and p of the classical system. Direct coexistence simulations were significantly longer (up to 10 million cycles) and Gibbs–Duhem simulations were typically ten times shorter. Further details of the path integral Monte Carlo simulations, for example, the rotational propagator, the acceptance criteria within the Markov chain, the evaluation of relative Euler angles between contiguous beads, can be found in ref. 32 and 33.

3 Results and discussion

To illustrate the methodology used in this work to determine the entire phase diagram of the quantum system, we shall

describe in detail the procedure used to determine the fluid–I_h coexistence curve:

- Determine the melting temperature $T_m^{\text{classical}}$ of the classical system at normal pressure.
- Determine the integral in eqn (5) by performing path integral NpT simulations for various values of λ' for ice I_h and for liquid water. For H₂O the values of $\lambda' = 1, 6/7, 5/7, 4/7, 3/7, 2/7, 1/7$ were used to evaluate this integral.
- Perform thermodynamic integration and determine the melting temperature T_m of the quantum system at which ice I_h and water have the same μ at normal p .
- Perform Gibbs–Duhem integration using path integral simulations to determine the full I_h–water coexistence line.

Free energy calculations for TIP4PQ/2005 yielded $T_m^{\text{classical}} = 282$ K for I_h ($p = 1$ bar). The same result 282 ± 3 K was obtained from direct coexistence simulations. In direct coexistence runs^{38,44} half of the simulation box is filled with ice and the other half with the liquid. NpT simulations at normal pressure are performed for several temperatures. For temperatures above the melting point the ice within the system melts, and for temperatures below the melting point the ice phase is seen to grow.

We then proceeded to calculate the integral in eqn (5) at normal p and $T = 282$ K (where the two phases have the same chemical potential in the classical system). To do this the mass of the atoms in the TIP4PQ/2005 “molecule” was incrementally increased by a factor of λ . Such a scaling only modifies the total mass of the molecule M and the eigenvalues of the inertia tensor (*i.e.* the principal moments of inertia), but leaves the geometry of the model and the location of the centre of mass unchanged. Seven scaling factors between $\lambda = 1$ and $\lambda = 7$ were used, and the corresponding exact rotational propagator at $T = 282$ K was calculated for each. Beyond $\lambda = 7$ the calculation of the propagator becomes prohibitively expensive to calculate, and a large number of simulations would be required to reduce the errors to an acceptable level. Path integral simulations were then performed, and the integrand of eqn (5) is determined (see Fig. 1a). The integral over the curve formed by these results provides the difference in excess quantum Gibbs energy between ice I_h and water, and therefore the difference in free energies between the two phases in the quantum system (for $T = 282$ K and $p = 1$ bar the two phases have the same chemical potential in the classical system). As can be seen in Fig. 1a the integrand for the liquid–I_h calculation is reasonably smooth and forms an almost horizontal line. For this reason it seems reasonable to extrapolate the integrand for $\lambda' < 1/7$ from the values obtained for larger λ' .

It can be seen that the kinetic energy of ice I_h is higher than that of water at 282 K and 1 bar, indicating that nuclear quantum effects are significantly larger in the ice I_h phase.⁴⁵ For rigid models nuclear quantum effects are related to the strength of the intermolecular interactions which, in the case of water, is dominated by hydrogen bonds. In ice I_h each molecule forms four hydrogen bonds with the first nearest neighbours, whereas in the liquid phase this number is somewhat smaller. The more “localised” character of the molecular libration in ice I_h with respect to the liquid leads to the higher kinetic energies observed. From the results shown in Fig. 1a it

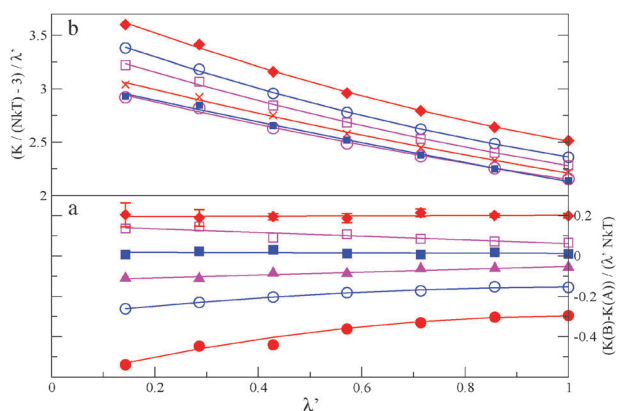


Fig. 1 (a) Integrand of eqn (5) (*i.e.* $(K_B - K_A)/(\lambda' NkT)$) as a function of λ' for transitions A–B. Key: red line with \blacklozenge is liquid–I_h at 282 K and $p = 1$ bar, magenta line with \square is II–V at 200 K and $p = 4112$ bar, blue line with \blacksquare is II–VI at 200 K and $p = 1$ bar, magenta line with \blacktriangle is V–VI at 200 K and $p = 9505$ bar, blue line with \circ is I_h–III at 200 K and $p = 3306$ bar, and the red line with \bullet is I_h–II at 200 K and $p = 1$ bar. Error bars (only shown for liquid–I_h) represent the standard error. (b) Integrand of eqn (4) for several ices at 200 K. Results were obtained using path integral simulations of the TIP4PQ/2005 model. The lines correspond to a fit of the simulation results to a second order polynomial. Results (from top to bottom) correspond to ice I_h at 3306 bar, ice III at 3306 bar, ice V at 4112 bar, ice II at 1 bar and ice VI at 1 bar. The integral of the curves (from 0 to 1) yields $G^{\text{ex},Q}/(NkT)$ which results in (from top to bottom) 3.11, 2.91, 2.80, 2.68, 2.60 and 2.59.

follows that μ of ice I_h in the quantum system is 0.20 kT higher than that of water at 282 K and 1 bar, indicating that the melting point of ice I_h in the quantum system is lower than that of the classical system. By using thermodynamic integration at constant p we found that at 258 K the chemical potential of the solid and fluid phases become identical. This value is the T_m of the quantum system. In order to corroborate this result, direct coexistence runs of the quantum system were undertaken. For the runs performed at $T = 266$ K and $T = 262$ K the total energy increases with time and reaches a plateau indicating the complete melting of the ice slab. At $T = 240$ K we saw a slow growth of the ice phase (see Fig. 2). At $T = 252$ K the energy was approximately constant along the run. This indicates that the melting point lies between $T = 252$ K and $T = 262$ K, thus we shall adopt the intermediate value of 257 K (± 5 K) in agreement with the free energy result of 258 K.

The entire I_h–water coexistence line is obtained by using the Gibbs–Duhem integration method. The Gibbs–Duhem integration method consists of a numerical integration of the Clapeyron equation and requires simply the knowledge of the enthalpy and volume difference between the two coexisting phases. The enthalpy of each phase is obtained from $H = K + U + pV$. Note that for each new temperature in the Gibbs–Duhem integration a propagator matrix must be calculated as the propagator depends on the value of PT . It can be seen that the I_h–water curve (Fig. 3) is essentially parallel to the experimental curve, shifted by ≈ 15 K due to the lower melting point of the TIP4PQ/2005 model. The aforementioned methodology for I_h–water was applied to the remaining phase equilibria,

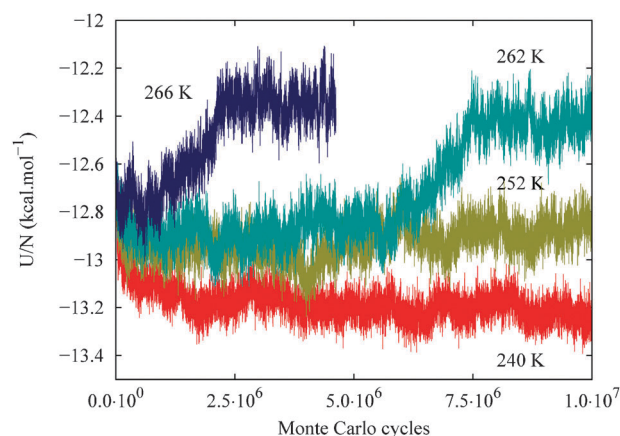


Fig. 2 Plot of the total potential energy (U) per particle from the liquid–I_h direct coexistence simulations of the quantum system at $p = 1$ bar.

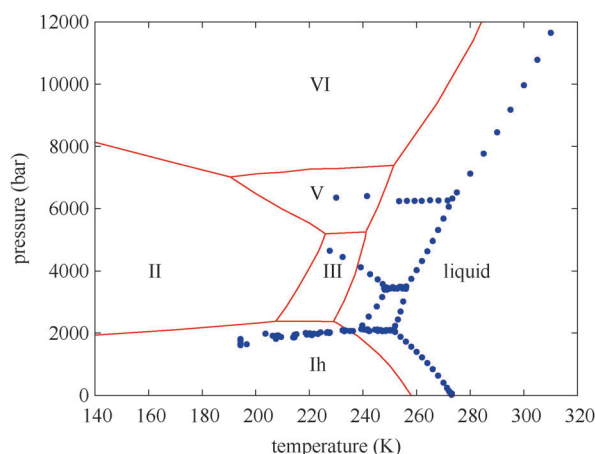


Fig. 3 Phase diagram of water from path integral simulations of the TIP4PQ/2005 model. Experimental results (blue points) are also shown.^{1,56}

leading to the complete phase diagram. A plot of the integrand of eqn (5) with respect to λ' is shown in Fig. 1a. The integral of these functions leads to the difference in excess quantum free energy between the two considered phases in units of NkT . As can be seen the integrand is rather smooth, and in most of the cases it can be well described by a straight line. It is worth noting that if this was always the case then one could obtain a reasonable estimate of the integral simply by obtaining the value of $\Delta K/(\lambda' NkT)$ at $\lambda' = 1/2$. In Fig. 3 the phase diagram of water as obtained from quantum simulations of the TIP4PQ/2005 model of water is presented and compared to the experimental phase diagram. One can see that the diagram is qualitatively correct, each phase is situated in the correct relation to the other phases. Furthermore, the gradients of the coexistence curves are also acceptable in comparison to experimental results. The most notable discrepancy is an overall shift of 15–20 K in the diagram to lower temperatures. In Fig. 4 the changes in volume along phase transitions obtained from the simulations are presented. It can be seen that they compare favourably with the experimental results obtained by Bridgman in 1912¹ (Fig. 4). Making use of a

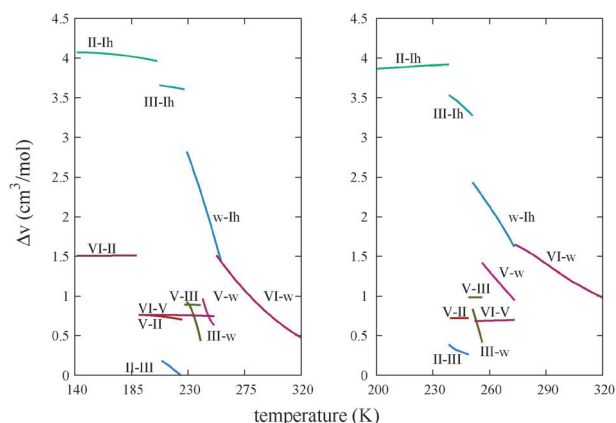


Fig. 4 Molar volume change ($\Delta v = v_B - v_A$) along the phase boundaries from (Left) path integral simulations and (Right) experimental results (w indicates the liquid phase).¹

recent publication by Loerting *et al.*⁴⁶ where the densities of ices I_h, II, III and V in the range of 77–87 K at normal pressure were determined using a methodology known as cryoflotation, we decided to study the densities at the intermediate temperature of 82 K. Additionally we also considered a couple of states for the liquid, and one for ice VI at room temperature. The results are summarised in Table 1. In general the simulation and experimental results coincide within 1%. Classical simulations of TIP4P/2005 tend to overestimate the experimental densities (at 82 K) by more than 3%.¹² Thus a quantum treatment is absolutely essential if one wishes to describe experimental results at low temperatures. The results of this table can also be used to estimate the value of the transition pressures at zero Kelvin as shown by Whalley.^{5,47} The estimates obtained in this way were consistent with those obtained from extrapolations to zero Kelvin of the coexistence lines. The maximum deviation found between the two methodologies was ≈ 700 bar, which is reasonable taking into account the combined uncertainty of all the calculations.

In order to highlight the differences between quantum and classical results for the phase diagram, the quantum and classical phase diagrams of the TIP4PQ/2005 model are superimposed in Fig. 5. Although the diagrams are qualitatively similar there are certain features of interest that can be observed. In the classical phase diagram the melting lines are

Table 1 Densities of ices and liquid water (in g cm^{-3}) under different thermodynamic conditions. All results were obtained for $p = 1$ bar, except the two labelled with an asterisk for which $p = 15400$ bar. Experimental densities for ice III correspond to the experimental values for ice IX the proton ordered form of ice III. Experimental results are from ref. 46, 58–60. The average values of U and K obtained from simulations (kcal mol^{-1}) are also shown

Phase	$T(\text{K})$	$\rho(\text{sim.})$	$\rho(\text{exp.})$	U	K
I _h	82	0.927	0.932	-14.302	1.914
II	82	1.189	1.211	-14.136	1.774
III	123	1.185	1.190	-14.046	1.837
III	82	1.148	1.169 ⁴⁶ , 1.160 ⁵⁷	-14.040	1.863
V	82	1.252	1.249	-13.883	1.808
VI	82	1.335	1.335	-13.745	1.790
VI(*)	300	1.383	1.391	-13.055	2.475
Liquid(*)	300	1.312	1.311	-11.997	2.395
Liquid	300	0.997	0.996	-11.897	2.366

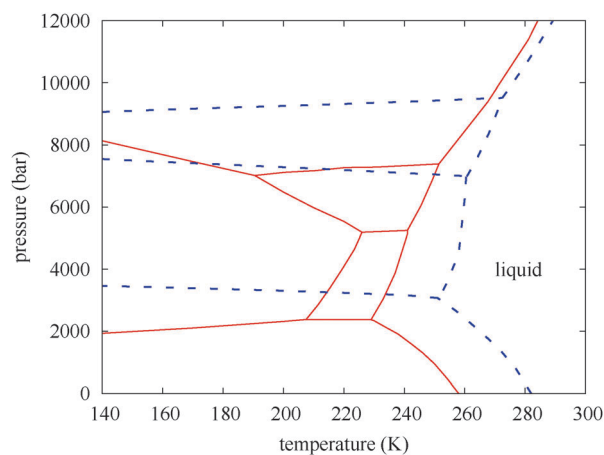


Fig. 5 Classical phase diagram of the TIP4PQ/2005 model (dashed blue lines) compared to the diagram obtained from path integral simulations (solid red lines).

shifted to higher temperatures, and solid–solid transitions are shifted to higher pressures (for a given temperature) with respect to the quantum phase diagram. Another important difference between the classical and quantum phase diagrams is that the region of the phase diagram occupied by ice II is significantly reduced in the classical treatment. In fact in the classical system the ice II–III transition is shifted to much lower temperatures and ice II is stable only for temperatures below 80 K. This shrinking of the ice II phase is consistent with recent findings by Habershon and Manolopoulos⁴⁸ who found that in classical simulations of the q-TIP4P/F model⁴⁹ ice III occupies the region of stability of ice II. This indicates that nuclear quantum effects play a significant role in determining the region of stability of ice II in the phase diagram of water.

It would be useful to have a rational guide to understand the changes in the phase diagram observed when including nuclear quantum effects. For this purpose the integrand of eqn (4), which facilitates the determination of the quantum excess free energy, is shown in Fig. 1b at a temperature of 200 K. The average kinetic energy of a harmonic oscillator of mass $M = M_0/\lambda'$ and frequency $\nu = \sqrt{\lambda'}\nu_0$ is given by:⁵⁰

$$\langle K \rangle = \frac{h\nu_0}{4} \sqrt{\lambda'} \coth\left(\frac{h\nu_0}{2k_B T} \sqrt{\lambda'}\right). \quad (6)$$

Upon performing a Taylor series expansion about $\lambda' = 0$ one obtains:

$$\frac{\langle K \rangle - \frac{1}{2}k_B T}{\lambda'} = \frac{1}{24} \frac{(h\nu_0)^2}{k_B T} - \frac{1}{1440} \frac{(h\nu_0)^4}{(k_B T)^3} \lambda' + \mathcal{O}(\lambda')^2 \quad (7)$$

For the rigid water model used in this work, one can describe the solid phases by a set of $6N$ oscillators (*i.e.* phonons). By assuming a unique frequency, as in an Einstein like model, one arrives at:

$$\frac{\langle K \rangle / Nk_B T - 3}{\lambda'} = \frac{1}{4} \left(\frac{h\nu_0}{k_B T}\right)^2 - \frac{1}{240} \left(\frac{h\nu_0}{k_B T}\right)^4 \lambda' + \mathcal{O}(\lambda')^2 \quad (8)$$

Thus for the Einstein model the integrand of eqn (4) is well behaved and has both a finite value and a finite negative

slope at $\lambda' = 0$. The results presented in Fig. 1b are indeed consistent with this predicted behaviour. From Fig. 1b it is possible to estimate ν_0 from either the slope or the intercept, obtaining “Einstein” like frequencies between 550 cm^{-1} and 450 cm^{-1} depending on the phase. These are typical values for intermolecular librations in water, which are located between 50 cm^{-1} and 800 cm^{-1} . A recent study has shown that one can reproduce the heat capacity of ice I_h using a selection of six fundamental frequencies selected from this range.⁵¹ It is worth mentioning that the TIP4PQ/2005 model also does a good job of calculating C_p when used in path integral simulations.¹³ The excess quantum free energies are obtained from the integration of the results of Fig. 1b. It is evident that at 200 K nuclear quantum effects significantly influence the free energies of the solid phases of water. By comparing the results of ice II at both 1 and 4112 bar it is seen that the pressure increases the magnitude of nuclear quantum effects at a given temperature although the increase is small (0.08 in NkT units for the considered pressures). The relative ordering in which the excess free energy increases is $II \simeq VI$, V, III and finally I_h .

The tetrahedral order parameter, q_t ,^{52,53} was designed to measure the degree of tetrahedral ordering in liquid water: q_t is defined as:

$$q_t = \left\langle 1 - \frac{3}{8} \sum_{j=1}^3 \sum_{k=j+1}^4 \left(\cos(\theta_{j,i,k}) + \frac{1}{3} \right)^2 \right\rangle \quad (9)$$

where the sum is over the four nearest (oxygen) neighbours of the oxygen of the i -th water molecule. The angle $\theta_{j,i,k}$ is the angle formed by the oxygens of molecules j , i and k , oxygen i forming the vertex of the angle. The tetrahedral order parameter has a value of 1 for a perfect tetrahedral network, and 0 for an “ideal gas” of oxygen centres. We shall make use of this descriptor in order to try to rationalise our results. The value of q_t of each solid at $T = 200 \text{ K}$ was obtained by annealing the solid structure while keeping the equilibrium unit cell of the system. In Fig. 6, the excess free energy is plotted as a function of q_t for the proton disordered ices, namely I_h , III, V and VI at a pressure of around 3600 bar and a strong correlation is evident. Ice II has a large value, $q_t = 0.83$, however,

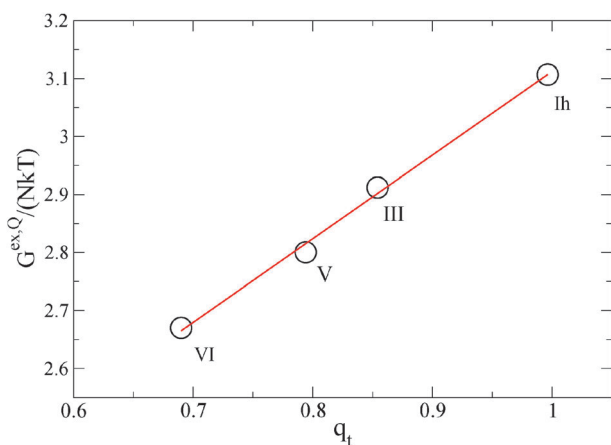


Fig. 6 Correlation between the excess quantum free energy and the tetrahedral order parameter for ices at 200 K and $p \approx 3600 \text{ bar}$. For ice VI the excess quantum free energy at 1 bar was increased by $0.08NkT$ to estimate its value at 3600 bar.

the impact of nuclear quantum effects on this ice phase is smaller than in the rest of the ice phases. Since ice II is the only proton ordered solid considered in this work, it is clear that in this case the fixed relative orientations between molecules are playing an important role in determining the magnitude of the nuclear quantum effects. It would be useful to evaluate the impact of nuclear quantum effects on the fluid phase. At 200 K the fluid is highly supercooled thus it is difficult to evaluate its $G^{\text{ex},Q}$. The difference between the total kinetic energy of a phase and that of the corresponding classical system under the same conditions also provides an estimate of the magnitude of nuclear quantum effects. One can see in Table 1 that at 300 K and 15400 bar the kinetic energy of liquid water is only slightly lower than that of ice VI. This indicates that the magnitude of nuclear quantum effects in the liquid is smaller than that of the ice with smallest nuclear quantum effects, ice VI. This is consistent with the low value, $q_t = 0.58$, of the tetrahedral order parameter found for the fluid phase at 300 K and 15400 bar.⁵⁴ It appears that the importance of nuclear quantum effects increases as the strength of the intermolecular hydrogen bonding increases. The strength of the hydrogen bonding seems to correlate (with the exception of ice II) with the value of the tetrahedral order parameter. For example, in ice I_h the first four nearest neighbours of a given molecule are located in a perfect tetrahedral arrangement which is the optimum situation to have a strong hydrogen bond. For the rest of the ices (and for water) the four nearest neighbours of a molecule form a distorted tetrahedron and therefore the strength of the hydrogen bond should decrease. The greater the strength of the hydrogen bond the higher the frequency associated with the librational mode, and therefore the higher the impact of nuclear quantum effects.

The change in the coexistence pressure for a certain temperature due to the inclusion of nuclear quantum effects can be approximated reasonably well by the expression

$$p - p_{\text{classical}} \simeq \frac{G_B^{\text{ex},Q} - G_A^{\text{ex},Q}}{V_B - V_A} \quad (10)$$

where the properties on the right hand side are evaluated at $p_{\text{classical}}$. It follows from eqn (10) that the impact of nuclear quantum effects on a given phase transition depends on the difference in the excess quantum free energy between the two phases, and on the volume change. The excess free energy difference between phases decreases in the following order: liquid- I_h , II- I_h , liquid-III, II-III, liquid-V, III- I_h , III-V, liquid-VI and finally II-VI. The impact of nuclear quantum effects on a certain phase transition will be small when the volume change of the phase transition is large, and large when the volume change is small. Volume changes along the phase transitions of water are presented in Fig. 4. Taking these two factors into account it is clear that the II-III phase transition is most affected by nuclear quantum effects (*i.e.* the excess free energy difference is large and the volume change is small), followed by the melting curves of ices (decreasing in the order liquid- I_h , liquid-III, liquid-V). This is followed by the transitions I_h -II, III-V and I_h -III. Finally the liquid-VI and the II-VI coexistence lines are those least affected by nuclear quantum effects.

4 Conclusion

This work illustrates that the calculation of the phase diagram of water, including nuclear quantum effects, is now feasible, although admittedly it is computationally expensive (even for the simple model considered in this work 8 CPUs were required for about 2 years to obtain the phase diagram presented). The impact of nuclear quantum effects on phase transitions is significant and can be rationalised in terms of the degree of tetrahedral ordering of the different phases and of the magnitude of the volume change involved in each phase transition. The TIP4PQ/2005 model yields a reasonable prediction of the experimental phase diagram of water. The simulation results are consistent with the Third Law of thermodynamics and predict rather well the densities of the different phases over a wide range of temperatures and pressures. With some delay with respect to the original contributors, this work shows that a simple modification of the water model proposed by Bernal and Fowler⁴¹ in 1933 can reproduce reasonably well the experimental phase diagram of water determined by Bridgmann¹ in 1912, providing results at low temperatures consistent with the Third Law first stated by Nernst in 1906.

In concluding this work it is worth commenting on the use of a rigid non-polarisable model to represent water. Naturally in reality water is both flexible and polarisable⁵⁵ so it goes without saying that this work is far from the last word on the matter, and the results presented here form only a way-point on the long road to obtaining a definitive model of water that describes all of the facets of this intriguing molecule. That said, path integral simulations of the TIP4PQ/2005 model have provided us with the best phase diagram of water calculated to-date.

Acknowledgements

This work was funded by grants FIS2010-16159 and FIS2010-15502 of the Dirección General de Investigación and S2009/ESP-1691-QF-UCM (MODELICO) of the Comunidad Autónoma de Madrid. The authors would like to thank Prof. J. L. F. Abascal for many helpful discussions.

References

- 1 P. W. Bridgman, *Proc. Am. Acad. Arts Sci.*, 1912, **XLVII**, 441.
- 2 C. G. Salzmann, P. G. Radaelli, E. Mayer and J. L. Finney, *Phys. Rev. Lett.*, 2009, **103**, 105701.
- 3 C. G. Salzmann, P. G. Radaelli, B. Slater and J. L. Finney, *Phys. Chem. Chem. Phys.*, 2011, **13**, 18468.
- 4 M. D. Morse and S. A. Rice, *J. Chem. Phys.*, 1982, **76**, 650.
- 5 E. Whalley, *J. Chem. Phys.*, 1984, **81**, 4087.
- 6 J. A. Barker and R. O. Watts, *Chem. Phys. Lett.*, 1969, **3**, 144.
- 7 A. Rahman and F. H. Stillinger, *J. Chem. Phys.*, 1971, **55**, 3336.
- 8 E. Sanz, C. Vega, J. L. F. Abascal and L. G. MacDowell, *Phys. Rev. Lett.*, 2004, **92**, 255701.
- 9 J. L. F. Abascal and C. Vega, *J. Chem. Phys.*, 2005, **123**, 234505.
- 10 C. Vega and J. L. F. Abascal, *Phys. Chem. Chem. Phys.*, 2011, **13**, 19663.
- 11 J. L. Aragones, L. G. MacDowell, J. I. Siepmann and C. Vega, *Phys. Rev. Lett.*, 2011, **107**, 155702.
- 12 C. McBride, C. Vega, E. G. Noya, R. Ramirez and L. M. Sesé, *J. Chem. Phys.*, 2009, **131**, 024506.
- 13 C. Vega, M. M. Conde, C. McBride, J. L. F. Abascal, E. G. Noya, R. Ramirez and L. M. Sesé, *J. Chem. Phys.*, 2010, **132**, 046101.
- 14 L. H. de la Peña and P. G. Kusalik, *J. Am. Chem. Soc.*, 2005, **127**, 5246.
- 15 G. S. Fanourgakis and S. S. Xantheas, *J. Chem. Phys.*, 2008, **128**, 074506.
- 16 J. A. Morrone and R. Car, *Phys. Rev. Lett.*, 2008, **101**, 017801.
- 17 F. Paesani and G. A. Voth, *J. Phys. Chem. B*, 2009, **113**, 5702.
- 18 M. Ceriotti, M. Parrinello, T. E. Markland and D. E. Manolopoulos, *J. Chem. Phys.*, 2010, **133**, 124104.
- 19 S. Habershon and D. E. Manolopoulos, *J. Chem. Phys.*, 2011, **135**, 224111.
- 20 R. P. Feynman, *Rev. Mod. Phys.*, 1948, **20**, 367.
- 21 M. J. Gillan, in *The path-integral simulation of quantum systems*, ed. C. R. A. Catlow, S. C. Parker and M. P. Allen, Kluwer, The Netherlands, 1990, vol. 293, chap. 6, pp. 155–188.
- 22 J. A. Barker, *J. Chem. Phys.*, 1979, **70**, 2914.
- 23 D. Chandler and P. G. Wolynes, *J. Chem. Phys.*, 1981, **74**, 4078.
- 24 F. Sedlmeier, D. Horinek and R. R. Netz, *J. Am. Chem. Soc.*, 2011, **133**, 1391.
- 25 D. de Sancho and R. B. Best, *J. Am. Chem. Soc.*, 2011, **133**, 6809.
- 26 E. G. Noya, C. Vega, L. M. Sesé and R. Ramirez, *J. Chem. Phys.*, 2009, **131**, 124518.
- 27 A. Wallqvist and B. J. Berne, *Chem. Phys. Lett.*, 1985, **117**, 214.
- 28 R. A. Kuharski and P. J. Rossky, *Chem. Phys. Lett.*, 1984, **103**, 357.
- 29 E. Curotto, D. L. Freeman and J. D. Doll, *J. Chem. Phys.*, 2008, **128**, 204107.
- 30 E. Asare, A.-R. Musah, E. Curotto, D. L. Freeman and J. D. Doll, *J. Chem. Phys.*, 2009, **131**, 184508.
- 31 M. H. Müser and B. J. Berne, *Phys. Rev. Lett.*, 1996, **77**, 2638.
- 32 E. G. Noya, C. Vega and C. McBride, *J. Chem. Phys.*, 2011, **134**, 054117.
- 33 E. G. Noya, L. M. Sesé, R. Ramirez, C. McBride, M. M. Conde and C. Vega, *Mol. Phys.*, 2011, **109**, 149.
- 34 D. Frenkel and A. J. C. Ladd, *J. Chem. Phys.*, 1984, **81**, 3188.
- 35 E. G. Noya, M. M. Conde and C. Vega, *J. Chem. Phys.*, 2008, **129**, 104704.
- 36 J. K. Johnson, J. A. Zollweg and K. E. Gubbins, *Mol. Phys.*, 1993, **78**, 591.
- 37 D. A. Kofke, *J. Chem. Phys.*, 1993, **98**, 4149.
- 38 C. Vega, E. Sanz, J. L. F. Abascal and E. G. Noya, *J. Phys.: Condens. Matter*, 2008, **20**, 153101.
- 39 T. L. Beck, in *Quantum contributions to free energy changes in fluids*, ed. C. Chipot and A. Pohorille, Springer-Verlag, Berlin, Germany, 2007, vol. 86, p. 389.
- 40 V. Buch, P. Sandler and J. Sadlej, *J. Phys. Chem. B*, 1998, **102**, 8641.
- 41 J. D. Bernal and R. H. Fowler, *J. Chem. Phys.*, 1933, **1**, 515.
- 42 L. Pauling, *J. Am. Chem. Soc.*, 1935, **57**, 2680.
- 43 J. L. Aragones, L. G. MacDowell and C. Vega, *J. Phys. Chem. A*, 2011, **115**, 5745.
- 44 C. Cazorla, M. J. Gillan, S. Taioli and D. Alfe, *J. Chem. Phys.*, 2007, **126**, 194502.
- 45 L. H. de la Peña, M. S. G. Razul and P. G. Kusalik, *J. Chem. Phys.*, 2005, **123**, 144506.
- 46 T. Loerting, M. Bauer, I. Kohl, K. Watschinger, K. Winkel and E. Mayer, *J. Phys. Chem. B*, 2011, **115**, 14167.
- 47 J. L. Aragones, E. G. Noya, J. L. F. Abascal and C. Vega, *J. Chem. Phys.*, 2007, **127**, 154518.
- 48 S. Habershon and D. E. Manolopoulos, *Phys. Chem. Chem. Phys.*, 2011, **13**, 19714.
- 49 S. Habershon, T. E. Markland and D. E. Manolopoulos, *J. Chem. Phys.*, 2009, **131**, 024501.
- 50 R. Ramirez and C. P. Herrero, *J. Chem. Phys.*, 2010, **133**, 144511.
- 51 K.-T. Wang and Q. M. Brewster, *Int. J. Thermodyn.*, 2010, **13**, 51.
- 52 P.-L. Chau and A. J. Hardwick, *Mol. Phys.*, 1998, **93**, 511.
- 53 J. R. Errington and P. G. Debenedetti, *Nature*, 2001, **409**, 318.
- 54 M. Agarwal, M. P. Alam and C. Chakravarty, *J. Phys. Chem. B*, 2011, **115**, 6935.
- 55 B. Santra, J. Klimes, D. Alfe, A. Tkatchenko, B. Slater, A. Michaelides, R. Car and M. Scheffler, *Phys. Rev. Lett.*, 2011, **107**, 185701.
- 56 O. Mishima and S. Endo, *J. Chem. Phys.*, 1980, **73**, 2454.
- 57 B. Kamb and A. Prakash, *Acta Crystallogr., Sect. B: Struct. Sci.*, 1968, **24**, 1317.
- 58 A. D. Fortes, I. G. Wood, M. Alfredsson, L. Vocadlo and K. S. Knight, *J. Appl. Crystallogr.*, 2005, **38**, 612.
- 59 A. Saul and W. Wagner, *J. Phys. Chem. Ref. Data*, 1989, **18**, 1537.
- 60 A. D. Fortes, I. G. Wood, L. H. Norman and M. G. Tucker, *ISIS Experimental Report*, 2010, **1010211**.